

Sub-diffraction Limit and Plasmonic Related Near-Field Lithography Using FDTD Algorithm

Abstract

The optical head for nanolithography, designed by the silver or gold nanometer-scale structures, can enhance and localize the electromagnetic field for specific optical spectrum in the small spatial regions because there are the surface waveguide modes or called the surface plasmons in the metal/dielectric structures. The optimization methods can be applied in the design procedures to tune the parameters of the structures and to improve the performance of the optical head. The designed structures can be fabricated by solid state techniques and can be measured by using the near field scanning optical microscopy. This proposed research can give more physical understanding about surface waveguide modes in metallic structures and the design procedures of the high-performance optical head for nanolithography. In general, there are various types of algorithm for electromagnetic simulation, such as rigorous coupled wave analysis (RCWA), differential method (DIM) and waveguide method (WGM), Finite-element modeling (FEM). RCWA, DIM and WGA are limited by slow convergence of Fourier series expansions, thus, RCWA, DIM and WGA are suitable for simulation in simple periodic 2D structure only. However, FDTD and FEM can both be applied to the structure that more complex and bigger. There are some limitations in computation due to the limited memory accessed on single desktop. For example, 8GB memory in one processor, the maximum simulation volume is a cube with its edge length 200nm for short wavelength. Thus, it is necessary to increase computation ability to deal with some structures which have larger volume and layout with more complexity structure. Base on this reason, MPI (Message Passing Interface) based FDTD parallel computing groundwork will be developed to increase both simulation speed and simulation size. There are still some computation techniques such as non-uniform grid method and Field decomposition method (Ex: Konstantinos Adam, Andrew R. Neureuther, "Simplified Models for Edge Transitions in Rigorous Mask Modeling," Proc. of SPIE Vol. 4346, 2001) to enhance computation ability. And field decomposition method can be considered after simulation groundwork being established.

Methods and Progress

To fulfill our goals to study and design the probe type and nanolens type optical head for nanolithography, we will simulate and optimize the structures. Also, we will compare these two types optical head in simulation and design several optimized structures for using in specific applications. Due to the facilities we can access, we plan to fabricate nanolens type optical head with small holes. We plan to use the first half year in analytical study and numerical simulation, and at the same time, the research assistants in this proposed research project will get the training to use the fabrication and measurement facilities. In the last half year in this proposed research project, we plan to have the fabrication and measurement for our optimized nanolens type optical head structure. We will use finite element method (FEM) and Finite difference time domain method (FDTD) to study the light propagation and localization in the probe type tips and nanolenses type optical head structures. We will also apply the parallel computing techniques in our programming

to simulate larger domain problem in PC Linux clusters which we can access in National Taiwan University and National Center for High-Performance Computing. We are familiar with 2-D FEM simulation for nanometer scale structure in Matlab environment, and we have the experiences for 3-D FEM simulation in the commercial software, like COMSOL Multiphysics and ANSOFT HFSS while PI studied his Ph. D. in the Department of Electrical Engineering, Purdue University. We will simulate the electromagnetic field in different shapes of dielectric and metal with consideration of distance from tips to circuit board which can have photoresist on its surface. The Ag or Au nanolenses structure are attached on the substrate, and they are integrated with light source, like laser or light emitting diode (LED). With a suitable design of the nanolenses device structure, the light can go through the aperture and have a strong focus spot in the circuit board for the application of nanolithography or nanoimaging. We will study the field transmission for the silver or gold structures. We choose Ag and Au in our proposed study because they have nice optical properties, low loss in optical spectrum, and the fabrication techniques by these metals are well-developed in semiconductor processing. It is the slot cases for 2-D structure and holes for 3-D structure, and there are conjugated surfaces around the slots or holes to enhance the field transmission. We will not only study the periodical conjugated surface but also non-periodical surface by optimizing the structure. We have the experiences in the optimization method as PI applied a multi-resolution optimization method in his previous study of the design of near-field irregular diffractive optical elements and investigation of the irregular etallic waveguides. In our experience, the device with optimized structure can have much better performance than the device without optimization. We believe that we can apply the same or similar optimization method in the nanolenses design. We will also investigate the performance of the nanolenses by considering the substrate material and thickness, the light source (laser or LED), and the effect of the position and material of the circuit board. We will also consider the effect from the fabrication errors, for example, the hole in the substrate layer is not a go-through hole. We will investigate all of these options numerically, with a view to future experiments. Designs will be studied for performance, sensitivity and consideration for fabrication.

A model for the influence of granularity in a negative refractive index lens

It is known that a negative refractive index slab provides for evanescent field amplitude amplification field amplification and the negative refractive index operating at microwave frequencies has been achieved by building an array of electric and magnetic dipoles, a metamaterial, and operating above the dipole resonances . The sub-wavelength image resolution is limited by loss in a negative refractive index slab . To understand the influence of dipole density of the metamaterial which has the negative refractive index, we establish a model for granularity and simulate different dipole density of the metamaterial. A finite element model for the scattering problem was used to find the spatial fields in image plane on one side of the slab with a point source located on the other side of the slab. We find that the bandwidth of the plane wave spectrum reduces as the dipole density decreases. Our model hints at the dipole density that will be needed in order to achieve significant improvement over the wavelength-limited imaging of positive index lenses. This research result will be presented in the 1st European Topical Meeting on Nanophotonics

and Metamaterials in 2007 . Irregular diffractive optical elements (IDOEs) offer a large number of degrees of freedom which can be used to control the desired spatial and temporal field transformation within the strong scattering near-field. We used the multi-resolution direct binary search method to optimize and design the dielectric irregular diffractive optical elements structures having sub-wavelength features that achieve near-field. focusing below the diffraction limit. We found that the sub-wavelength focal spots were possible because of evanescent field control exercised in the cost function and the focal plane being in the near-field, and that the size of the spot is limited only by the degrees of freedom in the structure. To find satisfactory solutions with acceptable computational effort, we used the discrete multi-resolution synthesis procedure, where coarse adjustments in the scattering geometry are followed by successively finer adjustments, and we found that this strategy was very useful in optimization procedures. Designs with a single focus, and two foci, depending on wavelength or polarization, illustrated the possible functionalities available from the large number of degrees of freedom. These examples suggested that the concept may find the applications in near-field lithography, wavelength division multiplexing, spectral analysis, and polarization beam splitters.

2D FDTD Algorithm

2D FDTD simulation groundwork has being developed during this month (TM wave with UPML boundary condition). Some details of this work are listed below:

Consider a region of that has no electric or magnetic current sources.

Faraday`s law

$$\nabla \times E = -\frac{\partial B}{\partial t} \quad (1)$$

Ampere`s law

$$\nabla \times H = \frac{\partial D}{\partial t} \quad (2)$$

E and H are vectors in three dimensions, but we consider only in two dimensions. We now show that properly defining a general constitutive tensor $\bar{\bar{s}}$ allows UPML medium to be used throughout the entire FDTD space lattice. This tensor provides for both a lossless isotropic medium in the primary computation zone, and individual UPML absorbers adjacent to the outer lattice boundary planes for mitigation of spurious wave reflections.

For matched condition, the time-harmonic Maxwell`s curl equations in the UPML can be written in the most general form as

$$\nabla \times \tilde{E} = -j\omega\mu_r\mu_0 s \tilde{H} \quad (3)$$

$$\nabla \times \tilde{H} = j\omega\mu_r\mu_0 s \tilde{E} \quad (4)$$

Where $\bar{\bar{s}}$ is a tensor defined by $\frac{s_x s_y}{s_z}$, and Ampere`s law in a matched UPML is expressed as

$$\frac{\partial \tilde{H}_y}{\partial x} - \frac{\partial \tilde{H}_x}{\partial y} = j\omega\epsilon_r\epsilon_0 \frac{s_x s_y}{s_z} \tilde{E}_z \quad (5)$$

Allowing for a non-unity real part κ , the multiplicative components of diagonal elements of \bar{s} are given by

$$s_x = k_x + \frac{\sigma_x}{j\omega\varepsilon_0} \quad s_y = k_y + \frac{\sigma_y}{j\omega\varepsilon_0} \quad s_z = k_z + \frac{\sigma_z}{j\omega\varepsilon_0} \quad (6-1,2,3)$$

Directly inserting (6) into (5) and then transforming into the time domain would lead to a convolution between the tensor coefficients and the E-field. A more efficient approach is to define the proper constitutive relationship to decouple the frequency-dependent terms.

Specifically, let

$$\tilde{D}_z = \varepsilon_r \varepsilon_0 \frac{s_y}{s_z} \tilde{E}_z \quad (7)$$

Then, (5) is rewritten as

$$\frac{\partial \tilde{H}_y}{\partial x} - \frac{\partial \tilde{H}_x}{\partial y} = j\omega s_x \tilde{D}_z \quad (8)$$

Now, we substitute s_x from (6), and then apply the inverse Fourier transform using the

identity $j\omega f(\omega) \rightarrow (\partial/\partial t)f(t)$. This yields an equivalent system of time domain differential equations for (8):

$$\frac{\partial \tilde{H}_y}{\partial x} - \frac{\partial \tilde{H}_x}{\partial y} = \frac{\partial}{\partial t} k_x D_z + \frac{1}{\varepsilon_0} \sigma_x D_z \quad (9)$$

The system of equations in (9) can be discretized on the standard Yee lattice. This leads to explicit time-stepping expressions for D_z

$$D_z \Big|_{i,j,k+1/2}^{n+1} = \left(\frac{2\varepsilon k_x - \sigma_x \Delta t}{2\varepsilon k_x + \sigma_x \Delta t} \right) D_z \Big|_{i,j,k+1/2}^n \quad (10)$$

$$+ \left(\frac{2\varepsilon \Delta t}{2\varepsilon k_x + \sigma_x \Delta t} \right) \left(\frac{H_y \Big|_{i+1/2,j,k+1/2}^{n+1/2} - H_y \Big|_{i-1/2,j,k+1/2}^{n+1/2}}{\Delta x} - \frac{H_x \Big|_{i,j+1/2,k+1/2}^{n+1/2} - H_x \Big|_{i,j-1/2,k+1/2}^{n+1/2}}{\Delta y} \right)$$

We consider (7) after multiplying both sides by s_x , and substituting s_x and s_z from (6-1,3), we have

$$\left(k_z + \frac{\sigma_z}{j\omega\varepsilon_0} \right) \tilde{D}_z = \varepsilon_r \varepsilon_0 \left(k_y + \frac{\sigma_y}{j\omega\varepsilon_0} \right) \tilde{E}_z \quad (11)$$

Multiplying both sides by $j\omega$ and transforming into the time domain leads to

$$\frac{\partial}{\partial t} (k_z D_z) + \frac{\sigma_z}{\varepsilon_0} D_z = \varepsilon_r \varepsilon_0 \left[\frac{\partial}{\partial t} (k_y E_z) + \frac{\sigma_y}{\varepsilon_0} E_z \right] \quad (12)$$

The time derivatives in (12) is discretized using standard Yee leapfrogging and time-averaging the loss term. This yields explicit time-stepping expressions for E_z . The E_z update is given by

$$E_z \Big|_{i,j,k+1/2}^{n+1} = \left(\frac{2\varepsilon k_y - \sigma_y \Delta t}{2\varepsilon k_y + \sigma_y \Delta t} \right) E_z \Big|_{i,j,k+1/2}^n \quad (13)$$

$$+ \left(\frac{1}{2\varepsilon k_y + \sigma_y \Delta t} \right) \left(\frac{1}{\varepsilon} \right) \left[(2\varepsilon k_z + \sigma_z \Delta t) D_z \Big|_{i,j,k+1/2}^{n+1} - (2\varepsilon k_z - \sigma_z \Delta t) D_z \Big|_{i,j,k+1/2}^n \right]$$

Also, from (2) and (4) we can get

$$\frac{\partial \tilde{E}_z}{\partial z} = -j\omega \mu_r \mu_0 \frac{s_y s_z}{s_x} \tilde{H}_x \quad (14-1)$$

$$\frac{\partial \tilde{E}_z}{\partial x} = j\omega \mu_r \mu_0 \frac{s_x s_z}{s_y} \tilde{H}_y \quad (14-2)$$

And, let

$$\tilde{B}_x = \mu_r \mu_0 \frac{s_z}{s_x} \tilde{H}_x \quad (15-1)$$

$$\tilde{B}_y = \mu_r \mu_0 \frac{s_x}{s_y} \tilde{H}_y \quad (15-2)$$

Then substitute s_x from (6), and then apply the inverse Fourier transform using the identity $\mathcal{F}^{-1}(\omega) \rightarrow (\partial/\partial t)f(t)$,

we can get (16-1,2) from (14-1,2)

$$\frac{\partial \tilde{E}_z}{\partial y} = -\frac{\partial}{\partial t} k_y B_x - \frac{1}{\varepsilon_0} \sigma_y B_x \quad (16-1)$$

$$\frac{\partial \tilde{E}_z}{\partial x} = \frac{\partial}{\partial t} k_z B_y + \frac{1}{\varepsilon_0} \sigma_z B_y \quad (16-2)$$

Explicit time-stepping expressions for B_x and B_y

$$\begin{aligned} B_x \Big|_{i,j+1/2,k+1/2}^{n+3/2} &= \left(\frac{2\varepsilon k_y - \sigma_y \Delta t}{2\varepsilon k_y + \sigma_y \Delta t} \right) B_x \Big|_{i,j+1/2,k+1/2}^{n+1/2} \\ &+ \left(\frac{2\varepsilon \Delta t}{2\varepsilon k_y + \sigma_y \Delta t} \right) \left(\frac{E_z \Big|_{i,j+1,k+1/2}^{n+1} - E_z \Big|_{i,j,k+1/2}^{n+1}}{\Delta y} \right) \end{aligned} \quad (17-1)$$

$$\begin{aligned} B_y \Big|_{i+1/2,j,k+1/2}^{n+3/2} &= \left(\frac{2\varepsilon k_z - \sigma_z \Delta t}{2\varepsilon k_z + \sigma_z \Delta t} \right) B_y \Big|_{i+1/2,j,k+1/2}^{n+1/2} \\ &+ \left(\frac{2\varepsilon \Delta t}{2\varepsilon k_z + \sigma_z \Delta t} \right) \left(\frac{E_z \Big|_{i+1,j,k+1/2}^{n+1} - E_z \Big|_{i,j,k+1/2}^{n+1}}{\Delta x} \right) \end{aligned} \quad (17-2)$$

Then, similar expressions can be derived for the remaining two H -field components as

$$\begin{aligned} H_x \Big|_{i,j+1/2,k+1/2}^{n+3/2} &= \left(\frac{2\varepsilon k_z - \sigma_z \Delta t}{2\varepsilon k_z + \sigma_z \Delta t} \right) H_x \Big|_{i,j+1/2,k+1/2}^{n+1/2} \\ &+ \left(\frac{1}{2\varepsilon k_z + \sigma_z \Delta t} \right) \left(\frac{1}{\mu} \right) \left[(2\varepsilon k_x + \sigma_x \Delta t) B_x \Big|_{i,j+1/2,k+1/2}^{n+3/2} - (2\varepsilon k_x - \sigma_x \Delta t) B_x \Big|_{i,j+1/2,k+1/2}^{n+1/2} \right] \end{aligned} \quad (18-1)$$

$$\begin{aligned} H_y \Big|_{i+1/2,j,k+1/2}^{n+3/2} &= \left(\frac{2\varepsilon k_x - \sigma_x \Delta t}{2\varepsilon k_x + \sigma_x \Delta t} \right) H_y \Big|_{i+1/2,j,k+1/2}^{n+1/2} \\ &+ \left(\frac{1}{2\varepsilon k_x + \sigma_x \Delta t} \right) \left(\frac{1}{\mu} \right) \left[(2\varepsilon k_y + \sigma_y \Delta t) B_y \Big|_{i+1/2,j,k+1/2}^{n+3/2} - (2\varepsilon k_y - \sigma_y \Delta t) B_y \Big|_{i+1/2,j,k+1/2}^{n+1/2} \right] \end{aligned} \quad (18-2)$$

Related Topic of Study

To fulfill our goals to study and design the probe type and nanolens type optical head for nanolithography, we will simulate and optimize the structures. Also, we will compare these two types optical head in simulation and design several optimized structures for using in specific applications. Due to the facilities we can access, we plan to fabricate nanolens type optical head with small holes. We plan to use the first half year in analytical study and numerical simulation, and at the same time, the research assistants in this proposed research project will get the training to use the fabrication and measurement facilities. In the last half year in this proposed research project, we plan to have the fabrication and measurement for our optimized nanolens type optical head structure. The detail procedures and progress are outlined as below.

Schedule in MPI based parallel computing:

1. Establishing simulation groundwork for parallel computing
 - a. Enormous structure
 - b. Complex structure

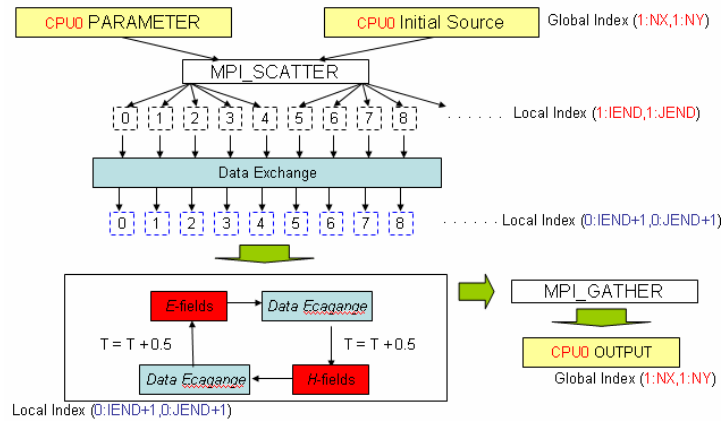


Fig. 1: MPI based parallel computing

The size of the simulation dimension is related to how much memory will be used, Typically, grid size of 200*100*200 meshes for a 3D FDTD simulation with 64-bit double precision needs about 1.152 GB memory. And For 8GB memory in one processor, if 20 meshes for one wavelength or 0.67nm per mesh for shorter wavelength, the computation limit is a cube with edge of 200nm.

Schedule in uniform and on-uniform grid method:

In diffractive optics, the rigorous domain typically refers to the regime where the feature sizes in the elements on the order of the wavelength of the incident light. At this scale, the assumptions inherent to scalar domain break down and effects based on polarisation, multiple scattering and the coupling of the electric and magnetic fields must be taken into account. Working on the rigorous domain we expect on developing techniques to efficiently and accurately simulate this propagation. These simulation techniques are necessary when modeling photonic crystal materials, high frequency gratings for chirped pulse compression and surface plasmon resonances and many other applications. The same time stepping algorithm as the FDTD method that differs from it in the way the fields are calculated. In this method, the electric and magnetic fields are co-located at a grid point, unlike the FDTD method where they are half a grid space apart. In addition to this, the differential equations are solved either by using a Fourier expansion, for periodic geometries. The advantage of the PSTD method over the FDTD method is that it is faster and remains stable for grid resolutions. In some cases, the FDTD method retains the advantage as it is not possible to implement non-uniform grids within the PSTD method using Fourier expansions, whereas it is possible within the FDTD method

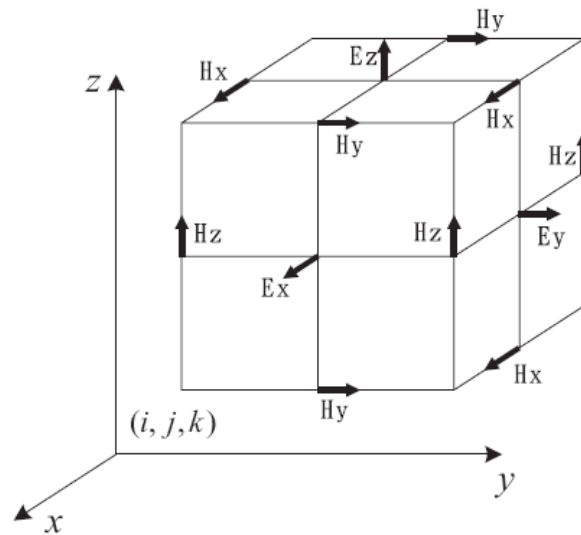
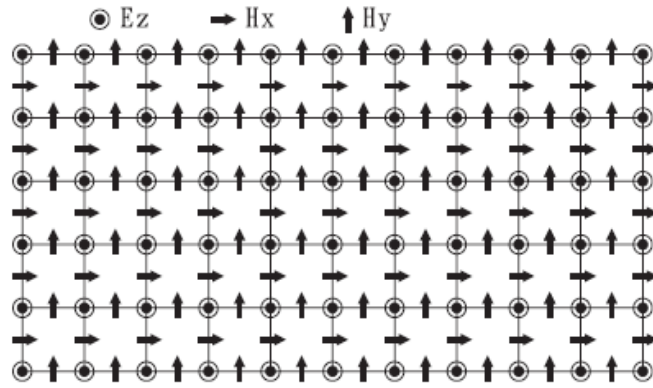


Fig. 2: Uniform grid

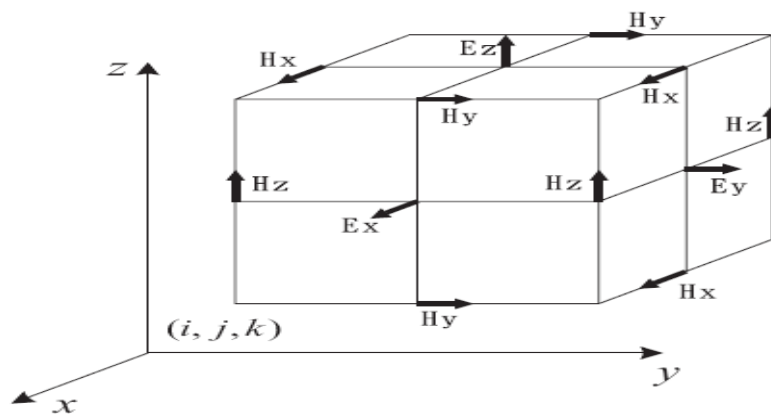
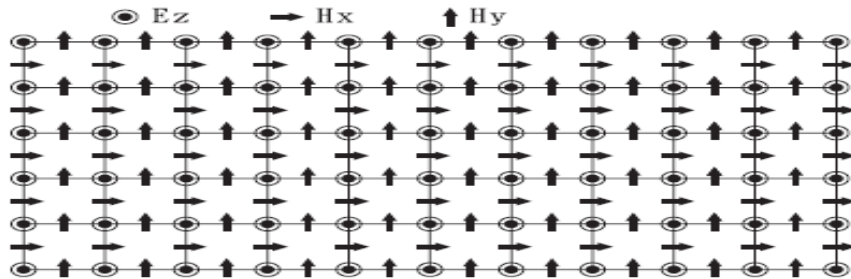


Fig. 3: Non-uniform grid

Conclusions

MPI (Message Passing Interface) based FDTD parallel computing groundwork will be developed to increase

both simulation speed and simulation size. There are still some computation techniques such as non-uniform grid method and Field decomposition method (Ex: Konstantinos Adam, Andrew R. Neureuther, "Simplified Models for Edge Transitions in Rigorous Mask Modeling," Proc. of SPIE Vol. 4346, 2001) to enhance computatoin ability. And field decomposition method can be considered after 3D simulation groundwork being established.

Selected Reference

- [1] J. Li, G. J. Burke, D. A. White, C. A. Thompson, and K. J. Webb, "Design of near-fieldirregular diffractive optical elements using a multiresolution direct binary search method," *Opt. Lett.* (2006).
- [2] M. Yang, J. Li, and K. J. Webb, "Functional waveguide mode transformers," *IEEE Trans. Microwave Theory Tech.* 52, 161–169 (2004).
- [3] M. Yang, J. Li, and K. J. Webb, "Functional field transformation with irregular waveguide structures," *Appl. Phys. Lett.* 83, 2736–2738 (2003).
- [4] K. J. Webb and J. Li, "Waveguide cavity surface-enhanced Raman scattering," *Phys. Rev. B* 73, 073404 (2006).
- [5] K. J. Webb and J. Li, "The electromagnetic basis for surface-enhanced Raman scattering," *Opt. Lett.* , under review process.
- [6] K. J. Webb and J. Li, "Analysis of transmission through small apertures in conducting films," *Phys. Rev. B* 73, 033401 (2006).
- [7] K. J. Webb and J. Li, "Resonant slot optical guiding in metallic nanoparticle chains," *Phys. Rev. B* 72, 201402 (2005).
- [8] E. Ozbay, "Plasmonics: merging photonics and electronics at nanoscale dimensions," *Science* 311, 189–193 (2006).